In Silico Characterization of Resonance Energy Transfer for Disk-Shaped Membrane Domains

Maria A. Kiskowski*† and Anne K. Kenworthy†‡
*Department of Mathematics, Vanderbilt University, Nashville, Tennessee 37240; †Department of Molecular Physiology and Biophysics, and ‡Department of Cell and Developmental Biology, Vanderbilt University School of Medicine, Nashville, Tennessee 37232

ABSTRACT Förster resonance energy transfer (FRET) has become an important tool to study the submicrometer distribution of proteins and lipids in membranes. Although resolving the two-dimensional distribution of fluorophores from FRET is generally underdetermined, a forward approach can be used to determine characteristic FRET "signatures" for interesting classes of microdomain organizations. As a first step toward this goal, we use a stochastic Monte Carlo approach to characterize FRET in the case of molecules randomly distributed within disk-shaped domains. We find that when donors and acceptors are confined within domains, FRET depends very generally on the density of acceptors within domains. An implication of this result is that two domain populations with the same acceptor density cannot be distinguished by this FRET approach even if the domains have different diameters or different numbers of molecules. In contrast, both the domain diameter and molecule number can be resolved by combining this approach with a segregation approach that measures FRET between donors confined in domains and acceptors localized outside domains. These findings delimit where the inverse problem is tractable for this class of distributions and reframe ways FRET can be used to characterize the structure of microdomains such as lipid rafts.

INTRODUCTION

Cell membranes contain localized regions of specialized lipid and protein composition known as membrane microdomains. Recently, much interest has been devoted to understanding the structural and functional properties of a class of membrane microdomains termed lipid rafts. Commonly defined as microdomains enriched in cholesterol and sphingolipids, lipid rafts are envisioned to function as platforms that concentrate and segregate proteins within the plane of the bilayer (1–3). The structure of such domains in intact cell membranes is still unclear, fueling controversies over the raft model (4). Except in specialized circumstances, lipid rafts in most cells cannot be directly viewed with light microscopy. Instead, the size of lipid rafts has been estimated as submicrometer in dimension. Current estimates suggest they may be as small as 5–10 nm and contain as few as three or four proteins (5).

Given the small size of lipid rafts, Förster resonance energy transfer (FRET) has become an important tool to study their properties in cell membranes (6–10). FRET reports on the proximity of two fluorescently labeled molecules separated by distances of <100 Å. Because of this, FRET can be used to test the hypothesis that raft proteins are enriched in domains with submicrometer dimensions. In such experiments, putative protein or lipid residents of membrane microdomains are typically labeled with FRET donor and acceptor fluorophores, and the resulting FRET is measured (11–19). The presence of FRET is not sufficient to provide evidence for the existence of domains because donors and acceptors confined to a membrane can readily be brought into FRET proximity by chance (20–22). Instead, the dependence of FRET on the surface density of the labeled molecules is assessed to provide a measure of the local packing of molecules in microdomains (reviewed by Kenworthy (7)).

An ultimate goal of these FRET measurements is the inverse problem of deducing the size of microdomains, the fraction of proteins localized to domains, the area fraction of membrane occupied by domains, and the mechanism of domain formation. Yet a pervasive feature of inverse problems is that solutions are not unique. Because transfer occurs between a pair of molecules, the only information that the FRET mechanism extracts from a fluorophore distribution is the distance between transferring molecules. In particular, the angles between segments connecting fluorophores are lost so that resolving the spatial arrangement of fluorophores is underdetermined. Thus, it is important to investigate which properties of a fluorophore distribution can be resolved using FRET in the context of the constraints placed on the distribution (i.e., in the case that some features of the distribution are already known).

Given the innate intractability of the inverse problem, how then can the underlying distribution of fluorophores be investigated? One approach to this question is to consider the forward problem by simulating FRET for biologically relevant distributions to fit experimental data (e.g., Sharma et al. (18)). Even the forward problem for FRET for an arrangement of fluorophores, in a plane or in space, is complex because of several nonlinear components in the calculation of the probability of transfer. First, the transfer rate between a donor-acceptor pair depends on the inverse of the separation distance raised to the sixth power. This results in a very sensitive

Submitted July 12, 2006, and accepted for publication January 17, 2007.

Address reprint requests to Anne K. Kenworthy, Department of Molecular Physiology and Biophysics, Vanderbilt University School of Medicine, Nashville, TN 37232. E-mail: anne.kenworthy@vanderbilt.edu.

0006-3495/07/05/3040/12 $2.00

doi: 10.1529/biophysj.106.093245

dependence on the separation distance: for small separations, a small change in distance results in a large change in the transfer rate. It is this nonlinear property that makes FRET successful as a spectroscopic ruler (23). A second source of nonlinearity is the effect of multiple acceptors, or ''acceptor competition.'' A third source of nonlinearity is the ''donor competition'' that results when multiple donors compete for transfer with acceptors in the same local area. Finally, in biological membranes, a very important source of nonlinearity results from the stochastic distribution of fluorophores. This last source of nonlinearity makes analytic treatment of FRET especially difficult. For certain limiting cases in which geometric constraints are imposed on fluorophore positions, for example, assuming a perfectly random distribution or noninteracting oligomers with fixed distances, FRET can be calculated analytically (20–22,24–28). Most biologically relevant distributions lie somewhere between these two extremes and are difficult or impossible to calculate analytically. Because the individual fluorophore interactions of FRET are entirely understood, an individual-based Monte Carlo model can be used to capture all relevant aspects of membrane FRET (29–31). We therefore use this approach to characterize FRET for a general class of membrane microdomain distributions in which molecules are randomly distributed within disk-shaped domains of fixed radius.

Theory of FRET for multiple acceptors

Fluorescence resonance energy transfer occurs when the absorption spectrum of a fluorophore (the acceptor) overlaps with the emission spectrum of another fluorophore (the donor) so that nonradiative transfer of the excitation energy occurs from the donor to the acceptor. The transfer rate k_t from a single donor to a single acceptor (the single-distance model (32)) can be expressed as a function of the separation distance R (for R in the 10- to 100-Å range), the donor lifetime τ_D, and the Förster distance R_0:

$$k_t = 1/\tau_D \times R_0^6/R^6. \quad (1)$$

The Förster distance R_0 is the critical separation distance at which excitation transfer occurs with 50% probability over the lifetime of the donor and depends, among other things, on the spectral overlap of the fluorophores and the relative orientations of their transition dipoles during the energy transfer process. A widespread measure of FRET is the FRET efficiency E, which can be robustly measured experimentally in several ways (29). The FRET efficiency is the ratio of the transfer rate to the total decay rate of the donor and can be calculated from Eq. 1 as:

$$E = R_0^6/(R_0^6 + R^6). \quad (2)$$

For the case of small oligomers in which there are two interacting molecules separated by a fixed distance (i.e., dimers), the FRET efficiency can be described with a relatively simple analytic expression using the single distance model. The average FRET efficiency within a dimer is equal to the probability of transfer from the donor to the second molecule (given that the second molecule is labeled with an acceptor) times the probability that the second molecule is labeled with an acceptor:

$$E_{dimer} = [R_0^6/(R_0^6 + R_{exc}^6)] \times f_A, \quad (3)$$

where R_{exc} is the donor-acceptor separation and f_A is the fraction of molecules that are labeled with acceptors.

For the application of FRET within biological membranes, the single-distance theory must be expanded to include the effects of multiple donors and multiple acceptors arranged in heterogeneous distributions. The earliest studies of FRET departing from the single-distance model studied FRET for several acceptors surrounding a single donor (33–35). In the case of weak dipole-dipole coupling, the rate of transfer from an excited donor to multiple acceptors separated at distances R_i is the sum of the individual transfer rates:

$$k_t = 1/\tau_D \Sigma (R_0/R_i)^6. \quad (4)$$

This description of the effect of multiple acceptors was first described by Förster (33).

In the case of trimers (oligomers with three molecules), the analytic expression for the average FRET efficiency is still straightforward but more complex because an excited donor may be oligomerized with one acceptor-labeled molecule (Case A) or two acceptor-labeled molecules (Case B). The transfer efficiency in Case A is the same as that for the dimer (Eq. 3). By Eq. 4, the transfer rate for Case B is $k_t = (1/\tau_D)$ $[(R_0/R_{exc})^6 + (R_0/R_{exc})^6]$ so that the FRET efficiency is $E = [2R_0^6/(2R_0^6 + R_{exc}^6)]$. Weighting by the probabilities of Case A and Case B, the FRET efficiency of a distribution of trimers is:

$$E_{trimer} = [R_0^6/(R_0^6 + R_{exc}^6)] \times 2f_A(1 - f_A) + [2R_0^6/(2R_0^6 + R_{exc}^6)] \times f_A f_A. \quad (5)$$

Note that whereas the effect of multiple acceptors on the transfer rate is linear because the total transfer rate equals the sum of each individual transfer rate (Eq. 4), the effect of multiple acceptors on the probability of transfer is nonlinear. For example, although two acceptors equidistant from a donor double the transfer rate compared to only one acceptor, the probability of transfer occurring with either acceptor is less than doubled. The effect of two acceptors on the probability of transfer can be understood by computing the probability of events that are not mutually exclusive. An acceptor separated at a distance R_{exc} from a donor has a transfer rate k_t that results in a probability P of transfer. Two acceptors separated at distance R from a donor have a sum transfer rate of 2 k_t. However, because the two acceptors compete for a single transfer, the probability of transfer is equal to the probability

that either acceptor transfers minus the joint probability J that they both transfer: $(P + P - J) < 2\ P$.

In 1964, Eisenthal and Siegel (24) considered more sophisticated consequences of multiple acceptors and multiple donors. Assuming an averaged distribution of random fluorophores in continuous space, they demonstrate analytically that the population of excited donors that undergo transfer is not distributed randomly in steady state. Rather, these donors are a population of donors that are near acceptors. Wolber and Hudson (21) elaborated on this model by considering distributions that account for the molecule exclusion radius. A consequence of multiple acceptors and donors borne by these analyses is that there is a multiplicity of donor molecule environments that independently contribute to FRET; for example, this results in a nonexponential fluorescence decay function (21). FRET values for random, homogeneous distributions have been calculated using analytic approximations (20–22,24,36) and through simulation approaches (29,31, 36). Small oligomers and the homogeneous random case occur as limiting cases of the disk-shaped domain model that we consider here. FRET for the intermediate case of small random domains has been considered by Sharma et al. (18).

MATERIALS AND METHODS

Stochastic model of FRET for disk-shaped domains

Our stochastic model of FRET is based on that of Berney and Danuser (29). The model simulates fluorophore excitation, decay, and resonance transfer as stochastic processes. FRET parameters are a static fluorophore distribution Φ, donor and acceptor lifetimes τ_D and τ_A, and the Förster length R_0. Each fluorophore is equipped with a Boolean state 0 or 1 that corresponds to the relaxed or excited state, respectively. Time is evolved in discrete time steps; each time step corresponds to Δt nanoseconds. The system may be considered a discrete memoryless Markov chain because the system at time step $t + 1$ depends only on the state of the system at time step t. Initially, all fluorophores are assigned the unexcited state 0. At each time step, the simulation implements the following rules:

1. Donor excitation: Donor excitation is modeled by assuming a light of constant intensity and wavelength so that an unexcited donor is excited with constant probability P_{excite} at each time step. The probability of excitation is equal for every unexcited donor, and more than one donor may be excited during a single time step. This probability summarizes the effects of membrane absorbance, the interaction of the donor with the excitation spectrum, the cross-sectional area of the donor, and the photon flux. If a donor is excited at the time step t, the donor state is updated from 0 to 1. As in Berney and Danuser (29), an ''exciton flux'' J is defined that is a measure of the number of photons reaching a donor per nanosecond. For a time step of length Δt nanoseconds, $J = P_{excite}$ / Δt. To simulate an arbitrarily small flux, excitation is modeled by taking $P_{excite} = 0$ if any acceptor or donor is excited and exciting exactly one donor in a random location when the system is entirely relaxed (all fluorophore states are '0'). We define the number of excitons as the number of times donors have been excited throughout the simulation, so each time a donor is excited, the number of excitons increases by 1.
2. Spontaneous donor decay: In the absence of any acceptors, the decay of an excited donor is modeled as stochastic, memoryless decay. For a donor lifetime τ_D, a donor decays with rate $k_D = 1/\tau_D$, which translates to a probability $P_D = \Delta t\ k_D = \Delta t\ /\tau_D$ of decay at each time step of length Δt. Note that the stochastic probability of decay has meaning only if the probability is <1. The time step length Δt should be chosen so that $\Delta t\ /\tau_D \ll 1$. If Y is the population size of excited donors, then the average change in this population as a result of decay is described by $\Delta Y = -Y\frac{\Delta t}{\tau_D}$. Taking the limit as $\Delta t \to 0$ and integrating, we recover the exponential decay equation $Y = Y_0 e^{\frac{-t}{\tau_D}}$. When a donor decays, its state is updated from 1 to 0.
3. Donor transfer and acceptor excitation: In the presence of free acceptors, the rate of donor deexcitation must include the rate of transfer with the rate of spontaneous decay k_D. The transfer rate k_T of an excited donor with a single acceptor at distance R is given by Eq. 1, and the transfer rate k_T in the case of more than one free acceptor is given by Eq. 4. The total rate of donor deexcitation is $k_{D+T} = k_D + k_T$, which translates to a total probability $P_{D+T} = \Delta t\ k_{D+T} = \Delta t\ (k_D + k_T)$ of donor deexcitation. As before, Δt should be chosen so that the probability of deexcitation $P_{D+T} \ll 1$. If deexcitation occurs at a time step, spontaneous decay or transfer occurs with normalized probabilities $k_D/(k_D + k_T)$ and $k_T\ /(k_D + k_T)$, respectively. In either case, the donor state is updated from 1 to 0. If transfer occurs, the ith acceptor is chosen for transfer with the normalized probability $((1/\tau_D)\times(R_0^6/R_i^6)/k_T$, and the state of the chosen acceptor is updated from 0 to 1.
4. Acceptor deexcitation: Acceptor decay is implemented in the same way as donor decay. The probability of acceptor decay at each time step is $\Delta t\ /\tau_A$.

Unless stated otherwise, in FRET simulations $\tau_D = \tau_A = 4$ ns, and the Förster length is 6.31 nm. Donors are excited in the limit when the flux $J \to 0$, so that there are no donor competition effects. We assume that the acceptor emission profile and the donor absorbance profile are well separated so there is no bleed-through excitation. In all simulations, the measured response variable is the FRET efficiency, defined as the total number of transfers divided by the total number of donor excitations. Simulations were scripted and run in Matlab (The MathWorks, Natick, MA). Our model simulates FRET for a given list of the x and y coordinates of N fluorophores and is available for download on request. The list of positions may be assigned randomly from initial conditions, may be scanned from an image of protein positions, or may be generated. A model that generates molecule coordinates for a number of common situations is available through Corry et al. (31). Their model also simulates FRET in two or three dimensions.

To simulate FRET for a given distribution of molecules, molecules are randomly labeled with donors and acceptors. Molecule positions are static throughout a simulation because we neglect the effect of diffusion. The effects of diffusion for conventional fluorophore lifetimes (i.e., those in the nanosecond range) are negligible (37). We define an intradomain FRET approach as the labeling method in which domain molecules are labeled with both acceptors and donors so that transfer occurs within domains. We define a segregation FRET approach as the labeling method in which domain molecules are labeled only with donors, although a second population of molecules located outside domains is labeled with acceptors so that FRET transfer occurs across the domain boundary. In either case, we assume that total acceptor fluorescence is measured during excitation at the donor excitation wavelength for different labeling scenarios (i.e., sensitized fluorescence (38–40)).

RESULTS

Disk-shaped domain model

We consider FRET for the class of distributions in which molecules are randomly distributed within identical, noninteracting disk-shaped domains. Each distribution within this class is described by the number of domains m, the domain radius r, the number of molecules per domain n, and the

exclusion radius of the molecules R_{exc}. The parameters r, R_{exc}, and n are the same for every domain within a single distribution. The molecule exclusion radius is modeled by imposing conditions that molecules cannot overlap and are completely contained within the domain. The intradomain molecule density δ^{Ω} is given by $n/\pi r^2$. The Ω superscript here and throughout this article indicates that the density is calculated within domains. As the intradomain density increases, by a decrease in the radius r or an increase in n, packing constraints result in increasingly nonrandom configurations. For example, when the molecule occupancy is 2, 3, or 7 and the domain radii are 5, 5.38, and 7.5 nm, respectively, packing constraints result in a nonrandom configuration in which molecules are fixed to positions on a hexagonal grid (Fig. 1 *Ai*). The separation between adjacent molecules is the exclusion radius. We define these three domains as oligomers because they are a fixed arrangement of n molecules where n is small (<10). An intermediate case occurs when the domain radius is small but large enough so that molecules position randomly within domains (Fig. 1 *Bi*). Finally, this class of distributions also includes distributions in which molecules are distributed over the entire membrane because this distribution occurs in the limit as $r \rightarrow \infty$. We define this as the homogeneous random case (Fig. 1 *Ci*).

Calculating local acceptor density

Because the interaction of donors with acceptors decreases by the inverse of the distance to the sixth power, FRET very generally depends on the number and distances of acceptors ''near'' donors, i.e., the distributions of acceptors within a small neighborhood of each donor (Eq. 4). For an arbitrary distribution, the most general definition of the neighborhood of each donor is a disk of radius $k R_0$ centered at each donor's location. In computational models of FRET, k has been taken to be 10 (29) or 6 (36). In this article, we study the extent to which FRET can be described as a function of a properly defined acceptor density within natural, self-defined domains. We define the intradomain acceptor density δ_A^{Ω} as the number of acceptors within domains divided by the area of domains. The A subscript here and throughout the article indicates that the acceptor density is calculated. The intradomain acceptor density is proportional to the number of acceptor-labeled molecules within the domain: $\delta_A^{\Omega} = nf_A/\pi r^2$, where f_A is the mole fraction of molecules that are labeled with acceptors. However, for small n this acceptor density does not reflect the acceptor density within domains reported on by FRET because of the conditional probability that at least one donor must be found within the domain. Thus, we consider the average acceptor density within a domain weighted by the number of donors in that domain, i.e., the donor-weighted intradomain acceptor density δ_{Aw}^{Ω}:

$$\delta_{Aw}^{\Omega} = \left(\Sigma_{i=1}^{m} \left(a_i/\pi r^2\right) d_i\right)/\Sigma_{i=1}^{N} d_i, \quad (6)$$

where a_i and d_i are the number of acceptors and donors in the ith domain and the sums are evaluated from $i = 1$ to $i = m$ where m is the total number of domains. For n randomly labeled molecules and a large number of domains m, δ_{Aw}^{Ω} is equal to the average density of acceptors in a domain given that there is a donor within the domain:

$$\delta_{Aw}^{\Omega} = (n-1)f_A/\pi r^2. \quad (7)$$

Throughout this article, we calculate the donor-weighted intradomain acceptor density using Eq. 7, and we refer to it as the local acceptor density. The global acceptor density δ_A (and the global molecule density δ) are defined as the total number of acceptors (or the total number of molecules) divided by the total membrane area.

Characterization of intradomain FRET for disk-shaped domains

Clustering of molecules within domains increases FRET efficiency relative to the case in which molecules are distributed randomly. We study how intradomain FRET depends on the spatial organization of molecules within domains by simulating FRET for oligomers, intermediate disk-shaped domains, and the homogeneous random case. For all cases, simulation results (Fig. 1) indicate that FRET efficiency increases with the global acceptor density because the FRET efficiency increases with the mole fraction of acceptor-labeled molecules (*A–Cii*) and decreases monotonically with the donor to acceptor ratio (*A–Ciii*). FRET efficiencies predicted by our simulation results for dimers and trimers and those calculated analytically are identical within simulation error (*Aii–iii*, *solid* versus *dotted lines*). This verifies that stochastic simulations agree well with analytic theory and, in particular, that the analytic equations capture all significant aspects of FRET for this simplified scenario. For homogeneous random domains, it has been previously established that the FRET efficiency increases with the density of acceptors (21,22, 29,31,36) and decreases with the ratio of donors to acceptors (29,31). For oligomers and disk-shaped domains, the results described in Fig. 1 are independent of the global molecule density because we assume that domains do not interact. However, the assumption that domains do not interact is valid only if the global molecule density is sufficiently low. Notice that the FRET efficiencies for the homogeneous case are comparable to those of oligomers when the global molecule density is 0.024 nm^{-2} because a density of 0.024 nm^{-2} is very high, comparable to the intradomain molecule density within oligomers. Generally, given a fixed global molecule density and a fixed number of domains, the FRET efficiency decreases systematically as the domain size increases (Fig. 2).

The simulation results described in Figs. 1 and 2 qualitatively indicate that FRET efficiency increases with the acceptor density within domains. This suggests that the ''FRET signature'' of disk-shaped domains may be characterized as a

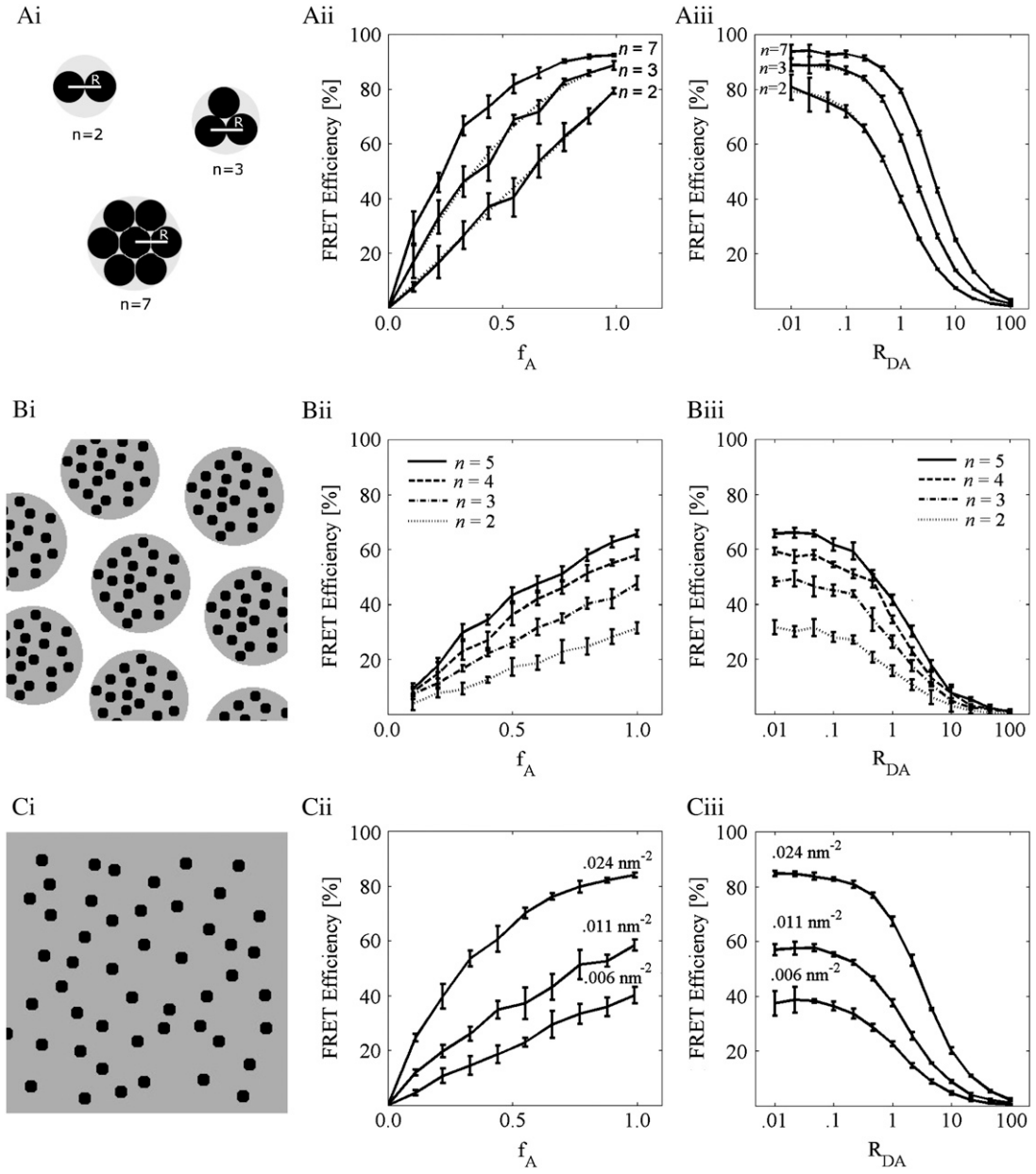

FIGURE 1 FRET dependence on spatial organization of molecules within disk-shaped domains. (*A–Ci*) Schematic depiction of disk-shaped domains for three classes of domains considered in this study: (*Ai*) oligomers, (*Bi*) intermediate domains, and (*Ci*) homogeneous random distributions (domain radius $r \rightarrow \infty$). (*A–Cii*) FRET dependence on mole fraction of acceptor-labeled molecules f_A for (*Aii*) dimers, trimers, and septamers, (*Bii*) intermediate domains, and (*Cii*) the homogeneous random distribution. The fraction of donor-labeled molecules is held constant at a low value ($f_D = 0.01$) while f_A is varied from 0 to 0.99. (*A–Ciii*) FRET dependence on ratio of donors to acceptors R_{DA} for (*Aiii*) dimers, trimers, and septamers, (*Biii*) intermediate domains, and (*Ciii*) the homogeneous random distribution. Molecules are labeled with either an acceptor with probability $f_A = (1 + R_{DA})^{-1}$ or as a donor with probability $1 - f_A$ so that molecule labeling is 100%. The dotted lines in (*Aii–iii*) show FRET for dimers and trimers using exact analytic expressions (Eqs. 3 and 5) and are equal to stochastic simulations within simulation error. For intermediate domains (*Bii–iii*), the domain radius $r = 10.6$ nm and the number of molecules per domain are increased from $n = 2$ to $n = 5$. For the homogeneous random case (*Cii–iii*), the global molecule density is 0.006, 0.011, or 0.024 nm^{-2}. For analytic and stochastic results, the molecule exclusion radius is 5 nm, and the Förster radius is 6.31 nm. Results of stochastic simulations for intradomain FRET are shown as mean and standard deviation of five independent simulations in which 2000 excitons are distributed among 5040 molecules and m domains where $m = 5040/n$.

function of FRET efficiency versus the local acceptor density. Fig. 3 *A* shows the dependence of FRET on the local acceptor density for all simulations described in Figs. 1 and 2. The FRET efficiency is aptly described as a single function of the local acceptor density because all simulation results may be estimated by the homogeneous random case reasonably well (*solid line*, Fig. 3 *A*). We define this curve as the ''intradomain FRET signature'' for disk-shaped domains when the particle exclusion radius and the Förster length are 5 nm and 6.31 nm, respectively. For different values of R_{exc}

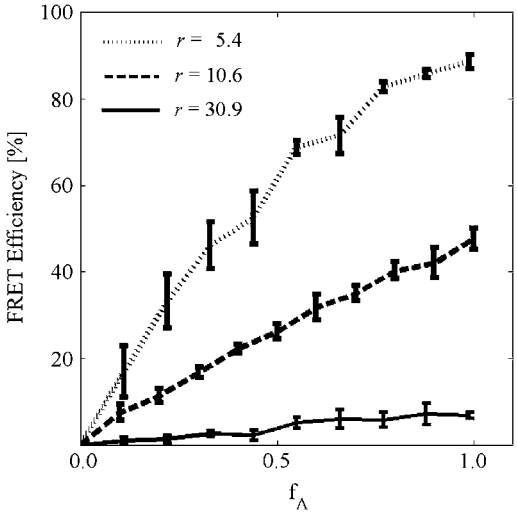

FIGURE 2 FRET dependence on spatial organization within domains when the global molecule density is held fixed at 0.001 nm^{-2}. FRET efficiency versus f_A when molecules are clustered within domains of three molecules with radius 5.4 nm (trimers, *dotted line*) or 10.6 nm (intermediate domains, *dashed line*) or distributed homogeneously (*solid line*). In each simulation 2000 excitons are distributed among m domains where $m = 5{,}040/n$ in a membrane area 2240 nm × 2240 nm. Note that, for comparison, in the homogeneous distribution, a disk-shaped region large enough to contain three molecules (on average) would have a radius of 30.9 nm. All other simulation parameters are as described in Fig. 1.

or R_0, the FRET signature is quantitatively different (Fig. 3 *B*). For a fixed R_{exc} and R_0 there is variability among simulations and variability in the relative positions of the curves so that the points vary within a region rather than lie along a curve. The extent of variation indicates the extent to which factors other than the local acceptor density affect FRET. We now describe some sources of this variability and explore their dependence on R_{exc} and R_0.

The local acceptor density is an important parameter for determining the FRET efficiency because it functionally summarizes the average number of acceptors near a donor and the average distance of those acceptors. However, FRET also depends on the distribution of donor-acceptor separations that are not entirely described by their average, apparent in the scatter of points in Fig. 3 for each FRET signature. One way that the distribution of donor-acceptor separations can be changed while maintaining a constant local acceptor density is by varying the extent of molecular crowding. The effects of molecular crowding independent of concentration effects were studied by Zimet et al. (36) in homogeneous distributions by simulating FRET for different values of R_{exc}. They found that crowding always increases FRET transfer rates and that the magnitude of this effect increases monotonically with the acceptor concentration.

Another way that crowding effects can be studied independently of acceptor concentration is by varying the extent of acceptor labeling for different molecule densities (compare Fig. 4, *A* and *B*). Fig. 4 *C* shows FRET efficiency versus local acceptor density for homogeneous distributions with different molecule densities for two different values of R_0. As did Zimet et al. (36), we find that crowding increases FRET efficiency and that the magnitude of these effects increases with the local acceptor density. Although the average donor-acceptor separations are the same, crowding biases the distribution of separations so that many separations are smaller than they would be otherwise. Variation in the FRET signature is also caused by differences among small oligomers (Fig. 3 *A*, *open black circles*) that would have the same amount of crowding. These differences in the FRET efficiency are largely a result of variation in the number of acceptors neighboring a donor, or neighbor effects. For example, in dimers the number of acceptors neighboring a donor may be 0 or 1, whereas for trimers the number of neighboring acceptors may be 0, 1, or 2. Even if parameters are chosen so that the average number of neighboring acceptors is the same, trimers will nevertheless have a wider distribution for the number of neighboring acceptors (compare Fig. 4, *D* and *E*). This explains the counterintuitive result that neighbor effects decrease the FRET efficiency for a constant local acceptor density. Fig. 4 *F* shows the extent of these effects as a variation in the FRET efficiency versus local acceptor density as the number of molecules per domain is increased within oligomers. Differences in the FRET efficiency caused

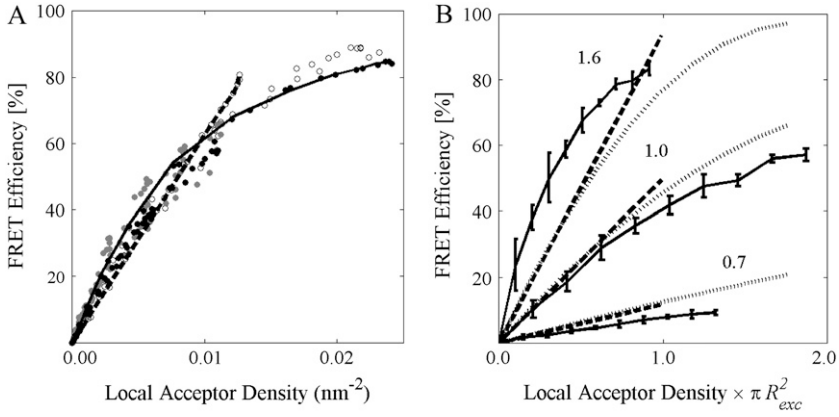

FIGURE 3 Intradomain FRET is described by local acceptor density. (*A*) FRET dependence on the local acceptor density for all simulations described in Fig. 1. Results for oligomers, intermediate domains, and homogeneous distributions are indicated with open black, solid gray, and solid black circles, respectively. Oligomer points when $n = 2$ are connected with a dashed line, and simulation results for a homogeneous random distribution of points for a global molecule density of 0.024 nm^{-2} are connected with a solid line. (*B*) FRET dependence on the local acceptor density normalized by πR_{exc}^2 for ratios $R_0 / R_{exc} = 0.7$ (3/4.2), 1.0 (5/5), or 1.6 (5.6/3.5) for dimers (*dashed lines*) and trimers (*dotted lines*) using the analytic equations described in Fig. 1 and for simulations for the homogeneous case when the global molecule density is 0.024 nm^{-2} (*solid lines*).

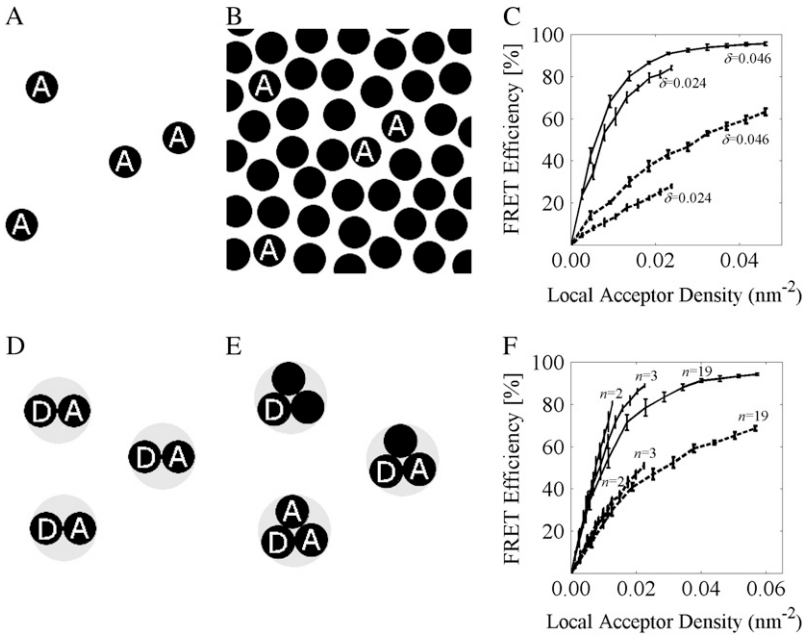

FIGURE 4 Systematic dependence of FRET on molecule crowding and the number of neighbors. (*A–B*) Schematic depiction comparing the spatial distribution of acceptors in the case of low (*A*) and high (*B*) molecule density for the homogeneous random case when the fraction of acceptor-labeled molecules is varied so that they have the same acceptor density (four acceptors per field). Although the global and local acceptor densities are the same, the distribution of donor-acceptor separations may vary as a result of the varied extent of molecule crowding. (*C*) FRET dependence on crowding effects in homogeneous domains; comparing global molecule density $\delta = 0.024$ nm^{-2} and $\delta = 0.046$ nm^{-2} when R_0 is 6.25 nm (*solid lines*) or 4.00 nm (*dashed lines*). For a given local acceptor density and R_0, differences in the curves are caused by crowding effects that result in increased ordering of molecules at higher density. (*D–E*) Schematic depiction comparing the distribution of the number of neighboring acceptors in dimers (*D*) and trimers (*E*). For both oligomers, the average number of acceptors neighboring a donor is the same (equal to 1.0), but the distribution of the number of neighboring acceptors is wider for the case of trimers. (*F*) FRET dependence on the number of molecules in hexagonally packed domains, comparing $n = 2$, $n = 3$, and $n = 19$ when R_0 is 6.31 nm (*solid lines*) or 5 nm (*dashed lines*). For a given local acceptor density and R_0, differences in the curves result from neighbor effects. For all simulations, the mole fraction of molecules labeled with donor is 0.01, and the molecule exclusion radius is 5 nm.

by neighbor effects increase systematically with increasing R_0 for $R_0 < 10$ nm (compare curves for two different values of R_0 in Fig. 4 *F*).

Implications of the intradomain FRET signature

Although our proposed FRET signature is expressed in terms of the local acceptor density, a parameter that cannot be experimentally measured, it nevertheless yields interesting implications. The FRET signature is monotonically increasing, so a measured value of FRET efficiency estimates a single value for the local acceptor density. As a result, it is straightforward to estimate the intradomain molecule density and the total domain area but difficult to determine the average domain radius. We illustrate these two points with two examples.

We assume that molecules distribute randomly within disk-shaped domains, and the particle exclusion radius and the Förster length are 5 nm and 6.31 nm, respectively, so that the FRET signature in Fig. 3 *A* may be used. We investigate the extent to which the size of domains, the fraction of membrane covered by domains, and the molecule density within domains can be determined.

For a given FRET efficiency, the local acceptor density $\delta^{\Omega}_{\mathrm{Aw}}$ can be estimated immediately using the FRET signature. The intradomain acceptor density $\delta^{\Omega}_{\mathrm{A}}$ (unweighted) can be estimated from $\delta^{\Omega}_{\mathrm{Aw}}$ using Eq. 7:

$$\begin{aligned}\delta^{\Omega}_{\mathrm{A}} &= \delta^{\Omega}_{\mathrm{Aw}} n/(n-1)\\ &\approx \delta^{\Omega}_{\mathrm{Aw}} \text{ when } n \text{ is large.}\end{aligned} \tag{8}$$

The domain fraction DF can be estimated by comparing the global acceptor density δ_{A} and the intradomain acceptor density $\delta^{\Omega}_{\mathrm{A}}$:

$$\begin{aligned}DF &= \text{global acceptor density}/\text{intradomain acceptor density}\\ &= \delta_{\mathrm{A}}/\delta^{\Omega}_{\mathrm{A}}\\ &= (\delta_{\mathrm{A}}/\delta^{\Omega}_{\mathrm{Aw}})\times[(n-1)/n)]\\ &\approx \delta_{\mathrm{A}}/\delta^{\Omega}_{\mathrm{Aw}} \text{ when } n \text{ is large.}\end{aligned} \tag{9}$$

This expression states that if the intradomain acceptor density and global acceptor density are similar, then the domain area and the membrane area are similar. Note that a precise estimate of the intradomain acceptor density depends on n so that $\delta_{\mathrm{A}}/\delta^{\Omega}_{\mathrm{Aw}}$ overestimates the domain fraction by a factor of $n\,/\,(n-1)$. As n becomes large, this factor approaches 1. Because the intradomain acceptor density is equal to the intradomain molecule density δ^{Ω} times the fraction of acceptor-labeled molecules ($\delta^{\Omega} = \delta^{\Omega}_{\mathrm{A}}/f_{\mathrm{A}}$), the intradomain molecule density may be estimated as $\delta^{\Omega} = \delta^{\Omega}_{\mathrm{Aw}}/f_{\mathrm{A}}$ when n is large.

We illustrate the applicability of these estimates in Fig. 5 *A*, which shows the estimated domain fraction versus the actual domain fraction for all simulations of the previous section. To estimate the domain fraction, we assumed that nothing other than the FRET efficiency and the global acceptor density for each simulation is measured from the distribution and use Eq. 9 to estimate the domain fraction. These results show that even without knowledge of the number of molecules per domain n, and with simulation error caused by stochastic fluctuations, the domain fraction can be

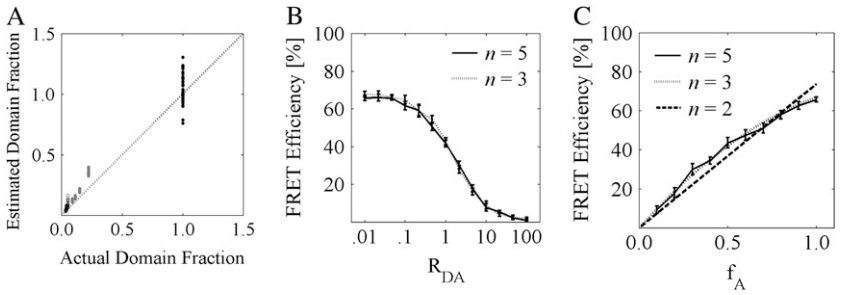

FIGURE 5 Delimiting the tractability of the inverse problem for intradomain FRET. (*A*) Estimated domain fraction versus actual domain fraction for all simulations described in Figs. 2 and 3. Points for oligomers, intermediate domains, and homogeneous random domains are open black, solid gray, and solid black circles, respectively. The estimated domain fraction is calculated for each simulation using Eq. 9. In each case, the local acceptor density δ^{Ω}_{Aw} is estimated for the simulated FRET efficiency by the solid line in Fig. 3 *A*. (*B*) The FRET efficiency versus donor/acceptor ratio for two distributions. In one distribution, *D1* (dotted line), the domain radius is 7.5 nm, and the number of molecules per domain is three. In the second distribution, *D2*, the domain radius is 10.5 nm, and the domain occupancy number is five molecules. The domain radius for each distribution was chosen to yield the same local acceptor density. Their domain fractions are 0.07 and 0.09, respectively. The molecule exclusion radius is 5 nm and the Förster radius is 6.31 nm. (*C*) When the particle exclusion radius is unknown, oligomers may be difficult to distinguish from larger domains. The solid line shows FRET efficiency versus mole fraction of acceptor-labeled molecules for intermediate domains when the domain radius is 10.6, the particle exclusion radius is 5 nm, and the number of molecules per domain is five. The dotted line shows the FRET efficiency for trimers using Eq. 5 for the particle exclusion radius that provides the closest fit to the FRET efficiency of intermediate domains ($R_{exc} = 6.29$ nm). The dashed line shows the FRET efficiency for dimers using Eq. 3 for the particle exclusion radius that provides the closest fit to the FRET efficiency of intermediate domains ($R_{exc} = 5.31$ nm).

estimated within an order of magnitude using this approach. Note that for all simulations, the same number of molecules is distributed within the same-sized region. Although the estimated domain fraction for domains with a small number of molecules per domain is overestimated by a factor of $n / (n - 1)$, the actual domain fraction in these cases is quite small so that this still yields a very good estimate. For homogeneous random domains, in contrast, small fluctuations in the estimated δ^{Ω}_{Aw} result in a larger range of predictions.

Although the domain fraction may be estimated, the domain radius is difficult to determine by intradomain FRET. To illustrate this point, we provide a concrete example (Fig. 5 *B*) in which two distributions *D1* and *D2* with different-sized domains cannot be distinguished even as the donor-to-acceptor ratio is varied over several orders of magnitude. Although the second distribution has more molecules, the domain radius r is also larger so that domains in both distributions have the same local acceptor density (Eq. 7). Note that because the distributions have the same FRET efficiency and the same global acceptor density, Eq. 9 would also predict equal domain fractions for the two distributions.

To this point, we have considered the inverse problem in the context of a known exclusion radius. If the exclusion radius is unknown, the domain fraction can be estimated by measuring the FRET efficiency at a constant global acceptor density while varying the domain organization (for example, via cholesterol depletion in the case of lipid rafts (12,15,16, 18,19)). However, multiple unknowns increase the extent to which the inverse problem for FRET is underdetermined. Fig. 5 *C* shows the FRET efficiency for intermediate domains when $n = 5$ and the particle exclusion radius is 5 nm (*solid line*) and for dimers (*dashed line*) and trimers (*dotted line*) for particle exclusion radii that minimize the difference in the curves. Although it may be possible to distinguish dimers by their linear dependence on the mole fraction of labeled acceptors, trimers with a particle exclusion radius of 5.31 nm cannot be distinguished from domains of five molecules with a particle exclusion radius of 5 nm.

A segregation-FRET approach provides an estimate of the disk-shaped domain radius for small and intermediate domain sizes

Because the domain radius cannot generally be resolved by FRET when donors and acceptors are located within the domain, we would like to find a labeling method that exploits the difference between domains with different radii. One approach to this problem is suggested by fluorescence quenching and FRET studies of membrane heterogeneity in vitro. To detect the presence of small domains, these studies measure segregation of donors and acceptors that occurs as the result of their association with separate phases (reviewed by Silvius and Nabi (10) and Heberle et al. (41)). We therefore designed a segregation-FRET simulation in which donors and acceptors are localized inside and outside of domains, respectively. This approach exploits the property of FRET that donor excitation occurs in a random donor position, whereas transfer occurs with the closest acceptor rather than with an acceptor in a random position. We postulated that when donors are confined within domains and acceptors are segregated outside domains (Fig. 6 *A*), this technique should provide a measure of the average domain radius.

We simulated segregation-FRET for domains of varying radii and found that the FRET efficiency decreases monotonically with domain radius so that domains may be clearly distinguished by their radii (Fig. 6 *B*, *solid line*). Smaller domains yield a higher FRET efficiency in this experimental scenario because the domain radius determines the scale of the average acceptor-donor separation. Further, the FRET efficiency does not depend on the density of donors within the domain. Although all domains had the same number of molecules, labeling 100% or 50% of the molecules in domains

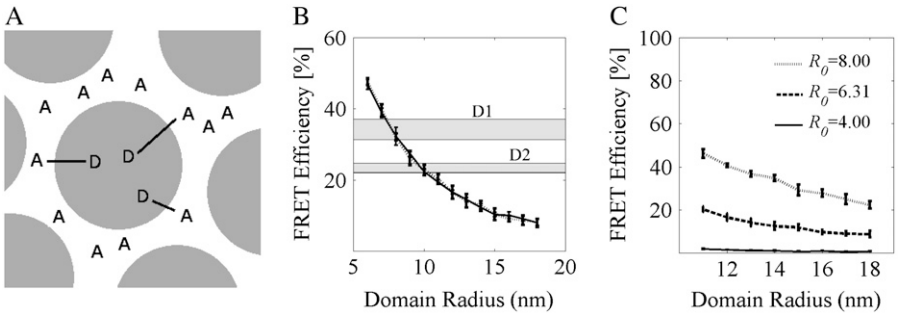

FIGURE 6 A segregation FRET method can determine domain radius independent of intradomain molecule density. (*A*) Labeling molecules within domains as donors and molecules outside domains as acceptors results in FRET transfer from molecules within the domain to molecules outside the domain. (*B*) The FRET efficiency versus domain radius using the segregation method when the fraction of donor-labeled molecules within domains is 1.0 (*solid line*) or 0.5 (*dotted line*). The Förster radius is 6.31 nm. The shaded horizontal regions indicate the range of simulated FRET efficiencies (within one standard deviation) when the segregation FRET method is applied to distributions *D1* and *D2* of Fig. 5 *B*. These regions predict domain radii of 7.5 ± 0.5 nm and 10.0 ± 0.5 nm, respectively. The actual domain radii were 7.5 and 10.5 nm, respectively. (*C*) The FRET efficiency versus domain radius when domain radii are distributed normally with a fluctuation of 25% (the fluctuation is defined as s^2/μ, the variance in domain radius s^2 divided by the mean domain radius μ) when the Förster radius is 4 nm (*solid line*), 6.31 nm (*dashed line*), or 8 nm (*dotted line*). For all simulations, 100 domains containing $n = 3$ randomly donor-labeled molecules are distributed in a 660 × 660 nm^{-2} area. The particle exclusion radius is 5 nm for all molecules, and the acceptor density was 0.024 nm^{-2} (outside domains). The range of domain radii in *C* is shifted compared to that in *B* to ensure that domains are large enough to accommodate three molecules given the normal fluctuation in domain radii. Simulation points and error bars show the average and standard deviation of five simulations in which 2000 excitons are simulated.

with donors had no effect on the FRET efficiency (*compare dotted and solid lines*, Fig. 6 *B*). Our disk-shaped domain model makes no assumptions about the mechanism of domain formation. However, it is likely that the radii of domains would vary to some extent in vivo. Fig. 6 *C* demonstrates that the segregation FRET method yields a predictive functional dependence on mean domain radius even in the case when the domain radius is allowed to fluctuate with a normal distribution (Fig. 6 *C*). This figure also shows that higher values of R_0 result in better resolution using this method; in particular, higher values of R_0 would be required to distinguish larger domain radii.

Combining FRET approaches

When the size of domains is unknown but the density of a molecule species outside the domains is known or can be estimated, the segregation approach can be used to infer the radius of domains. As an example, we consider the distribution *D1*, which could not be distinguished from distribution *D2* in Fig. 5 *B* and simulate segregation FRET for this distribution by labeling all domain molecules with donors and populating the nondomain space with acceptors for the same extradomain density that generated the curve in Fig. 6 *B*. The results of five independent FRET simulations yielded a FRET efficiency of 34 ± 3%. The range of simulated FRET efficiency within one standard deviation, indicated by the horizontal gray region in Fig. 6 *B*, predicts domains with a radius of 7.5 ± 0.5 nm. This prediction corresponds well to the actual domain radius of 7.5 nm. The FRET efficiency within one standard deviation for the distribution *D2* correctly predicts a larger domain radius of 10 ± 0.5 nm.

The radius estimated for distribution *D1* can be combined with the intradomain acceptor density measured by intradomain FRET to deduce the number of molecules in domains. The number of molecules in domains n can be derived from Eq. 7 if the local acceptor density δ^{Ω}_{Aw}, the domain radius r, and the fraction f_A of labeled acceptors are known:

$$n = \delta^{\Omega}_{Aw}\,\pi r^2/f_A + 1. \tag{11}$$

The intradomain FRET efficiency for distribution *D1* is 68 ± 1% when the donor to acceptor ratio is 0.01 (Fig. 5 *B*). This FRET efficiency predicts that δ_A is 0.011 ± 0.002 (Fig. 3 *A*). Because segregation-FRET estimates that r is 7.5 ± 0.5 nm, and f_A is 0.99 using $f_A = (1 + R_{DA})^{-1}$, Eq. 11 indicates there are 2.4 to 3.6 molecules per domain. This is an accurate estimate of the known number of three molecules per domain.

DISCUSSION

FRET measurements describe a distribution of acceptors and donors as a single point (e.g., the FRET efficiency) or a single curve (e.g., the FRET efficiency versus mole fraction of acceptor-labeled molecules). In either case, most of the information about the distribution is lost. Fortunately, this problem is ameliorated by the fact that we do not need to resolve every fluorophore position but instead are interested in average properties such as whether donors and acceptors are randomly distributed within domains, the intradomain density, and the domain size in the context of a constrained, biologically relevant subset of molecular distributions. In the current study we undertook a Monte Carlo–based approach to study the FRET signature of molecules randomly distributed within domains. For comparison with recent estimates of the size of lipid rafts (18,42), we focused on domains with radii ranging from 5 to 10.55 nm and assigned n = 2–7 molecules and also considered unbounded domains that would correspond to homogeneous distributions within the membrane. Our disk-shaped domain model includes oligomers in which the molecule separation is determined by the

molecule exclusion radius but excludes other types of nonrandom molecule configurations.

Limitations of this approach

In our stochastic model for FRET, we have made two approximations. First, we assume a fixed value for the Förster radius R_0 corresponding, for example, to the average value of R_0 measured experimentally. However, the value of R_0 actually varies stochastically for each pair of fluorophores in the membrane because R_0 is linearly proportional to the orientation factor κ^2 of each fluorophore pair (37). The orientation factor depends on how fluorophores are bound within the membrane and their rotational freedom within the membrane. For molecules that are freely rotating at speeds that are fast compared to the timescale of transfer, the average orientation factor can be estimated as two-thirds (43). Berney and Danuser (29) found a significant difference in their simulation results and a better prediction of their experimental results if they assumed a random orientation factor. Generally, the distribution of values for κ^2 and the distribution of values for R_0 are difficult to estimate and thus represent an additional important unknown. A recent study by Corry et al. (44) describes a scheme that can be used to place limits on the mean and distribution of this value experimentally. Second, we excluded the effects of donor competition by allowing the simulation to relax completely between donor excitations. Donor competition occurs when donors compete to transfer with available acceptors (29,31) and increases with photon flux because a higher photon flux increases the probability that two nearby donors will be simultaneously excited (31). Experimentally, a zero exciton flux corresponds to excitation at a low enough intensity that the probability of two nearby donors becoming simultaneously excited is negligible. It has been found by Corry et al. (31) that the effects of donor competition effects are negligible for typical, low laser irradiance.

Intradomain FRET

Intradomain FRET for small oligomers, intermediate domains, and homogeneous random distributions all exhibited a similar dependence on the local acceptor density defined using Eq. 7 (Fig. 3). This characterization consolidates a broad range of results into a single description and clearly defines the limitations of FRET measurements for this method and class of domains. For example, implications of this result are that the intradomain molecule density (and the domain fraction) may be estimated using intradomain FRET if the particle exclusion radius is known, although the domain radius (and/or the number of molecules per domain) is underdetermined (Fig. 5). Perhaps more surprising is the implication that domains of different sizes may yield the same FRET efficiencies if they have similar intradomain densities (Fig. 5 *B*).

Broadly, the domain fraction is estimated by comparing the estimated intradomain acceptor density with the measured global acceptor density. If the intradomain acceptor and global acceptor densities are equal, then the data are consistent with a homogeneous distribution in which the domain area is equal to the membrane area. Concentration of donors and acceptors in domains will lead to an intradomain acceptor density that is larger than the global acceptor density and results in the calculation of a smaller domain fraction. Meyer et al. used this reasoning to deduce that fluorescently tagged G protein-coupled receptors were concentrated within a domain fraction comprising $\sim$1% of the cell membrane (45).

We propose that the dependence of FRET on the local acceptor density defined as in Eq. 7 can be used as the ''FRET signature'' of the disk-shaped domain model in which molecules with an exclusion radius R_{exc} are randomly distributed within disk-shaped domains of radius r. The FRET signature may be generated with simulations if the exclusion radius R_{exc} and the Förster length R_0 are known. In our disk-shaped domain model, we assumed that domains within a single distribution are uniform in size and are spaced at sufficiently large distances so that they do not interact. We additionally assumed that no free monomers are present and that both the number of domains and number of molecules within domains are constant for a given distribution. Different models of domain organization will yield different FRET signatures. Further, we have demonstrated that effects such as variability in the number of neighbors and the extent of molecular crowding cause variation in the curve describing this dependence. Although the magnitude of these effects generally reduces the extent to which the domain fraction and molecule density can be estimated using the methods described here, these effects could possibly be used to extract more information from a distribution. For example, the different sized domains that could not be distinguished in Fig. 5 *B* may be better resolved by exploiting multiple neighbor effects (Fig. 4 *F*), and the oligomers and intermediate domains that could not be distinguished in Fig. 5 *C* may be better resolved by exploiting crowding effects (Fig. 4 *C*).

Segregation as a tool to characterize domain radius

Given the limit on the potential of intradomain FRET to report on the radii of disk-shaped domains, it is interesting to note that the majority of previous FRET studies of lipid rafts in cell membranes, including our own, have focused mainly on FRET measurements of donors and acceptors that should colocalize within lipid rafts (11–19). We show here that a segregation approach can resolve domain radius when the domain radius is less than three to four Förster lengths. Thus, a combination of segregation-based and intradomain-based FRET measurements will give a more comprehensive picture of domain structure and can be used as we have here to

robustly deduce the domain size, intradomain density, and the number of molecules within domains of a given distribution.

The application of segregation FRET to determine domain radii requires that donors be randomly distributed within disk-shaped domains, whereas acceptors are randomly distributed outside domains. The donor density within domains need not be known, but the acceptor exclusion radius and acceptor density must be known to quantitatively generate the dependence of FRET on the domain radius with simulations (data not shown). Intradomain and segregation FRET can be combined to estimate the domain radius, intradomain density, and number of molecules per domain if additionally the exclusion radius of molecules within domains is known. The results presented here provide a strong case for simultaneous simulation and experiment. Simulations can be designed to accommodate the specific set of known and unknown parameters for each experimental scenario and can help interpret experimental results in the complex context of stochastic FRET, stochastic molecule distributions, and systematic errors propagated by each parameter estimation.

We thank Drs. Berney and Danuser for generously providing Matlab scripts for their Monte Carlo FRET simulations.

Supported by the Vanderbilt Biomath Study Group and the National Institutes of Health (R01 GM073846 to A.K.).

REFERENCES

1. Simons, K., and W. L. Vaz. 2004. Model systems, lipid rafts, and cell membranes. *Annu. Rev. Biophys. Biomol. Struct.* 33:269–295.
2. Edidin, M. 2003. The state of lipid rafts: from model membranes to cells. *Annu. Rev. Biophys. Biomol. Struct.* 32:257–283.
3. Simons, K., and E. Ikonen. 1997. Functional rafts in cell membranes. *Nature.* 387:569–572.
4. Munro, S. 2003. Lipid rafts: elusive or illusive? *Cell.* 115:377–388.
5. Hancock, J. F. 2006. Lipid rafts: contentious only from simplistic standpoints. *Nat. Rev. Mol. Cell Biol.* 7:456–462.
6. Jacobson, K., and C. Dietrich. 1999. Looking at lipid rafts? *Trends Cell Biol.* 9:87–91.
7. Kenworthy, A. K. 2002. Peering inside lipid rafts and caveolae. *Trends Biochem. Sci.* 27:435–438.
8. Lagerholm, B. C., G. E. Weinreb, K. Jacobson, and N. L. Thompson. 2005. Detecting microdomains in intact cell membranes. *Annu. Rev. Phys. Chem.* 56:309–336.
9. Rao, M., and S. Mayor. 2005. Use of Forster's resonance energy transfer microscopy to study lipid rafts. *Biochim. Biophys. Acta.* 1746: 221–233.
10. Silvius, J. R., and I. R. Nabi. 2006. Fluorescence-quenching and resonance energy transfer studies of lipid microdomains in model and biological membranes. *Mol. Membr. Biol.* 23:5–16.
11. Kenworthy, A. K., and M. Edidin. 1998. Distribution of a glycosylphosphatidylinositol-anchored protein at the apical surface of MDCK cells examined at a resolution of <100 Å using imaging fluorescence resonance energy transfer. *J. Cell Biol.* 142:69–84.
12. Varma, R., and S. Mayor. 1998. GPI-anchored proteins are organized in submicron domains at the cell surface. *Nature.* 394:798–801.
13. Kenworthy, A. K., N. Petranova, and M. Edidin. 2000. High-resolution FRET microscopy of cholera toxin B-subunit and GPI-anchored proteins in cell plasma membranes. *Mol. Biol. Cell.* 11:1645–1655.
14. Kovbasnjuk, O., M. Edidin, and M. Donowitz. 2001. Role of lipid rafts in Shiga toxin 1 interaction with the apical surface of Caco-2 cells. *J. Cell Sci.* 114:4025–4031.
15. Zacharias, D. A., J. D. Violin, A. C. Newton, and R. Y. Tsien. 2002. Partitioning of lipid-modified monomeric GFPs into membrane microdomains of live cells. *Science.* 296:913–916.
16. Nichols, B. J. 2003. GM1-containing lipid rafts are depleted within clathrin-coated pits. *Curr. Biol.* 13:686–690.
17. Glebov, O. O., and B. J. Nichols. 2004. Lipid raft proteins have a random distribution during localized activation of the T-cell receptor. *Nat. Cell Biol.* 6:238–243.
18. Sharma, P., R. Varma, R.C. Sarasij, Ira, K. Gousset, G. Krishnamoorthy, M. Rao, and S. Mayor. 2004. Nanoscale organization of multiple GPI-anchored proteins in living cell membranes. *Cell* 116:577–589.
19. Hess, S. T., M. Kumar, A. Verma, J. Farrington, A. Kenworthy, and J. Zimmerberg. 2005. Quantitative electron microscopy and fluorescence spectroscopy of the membrane distribution of influenza hemagglutinin. *J. Cell Biol.* 169:965–976.
20. Fung, B. K., and L. Stryer. 1978. Surface density determination in membranes by fluorescence energy transfer. *Biochemistry.* 17:5241–5248.
21. Wolber, P. K., and B. S. Hudson. 1979. An analytic solution to the Förster energy transfer problem in two dimensions. *Biophys. J.* 28:197–210.
22. Dewey, T. G., and G. G. Hammes. 1980. Calculation of fluorescence resonance energy transfer on surfaces. *Biophys. J.* 32:1023–1035.
23. Stryer, L. 1978. Fluorescence energy transfer as a spectroscopic ruler. *Annu. Rev. Biochem.* 47:819–846.
24. Eisenthal, K. B., and S. Siegel. 1964. Influence of resonance transfer on luminescence decay. *J. Chem. Phys.* 41:652–655.
25. Veatch, W., and L. Stryer. 1977. The dimeric nature of the gramicidin A transmembrane channel: conductance and fluorescence energy transfer studies of hybrid channels. *J. Mol. Biol.* 113:89–102.
26. Adair, B. D., and D. M. Engelman. 1994. Glycophorin A helical transmembrane domains dimerize in phospholipid bilayers: a resonance energy transfer study. *Biochemistry.* 33:5539–5544.
27. Moens, P. D., D. J. Yee, and C. G. dos Remedios. 1994. Determination of the radial coordinate of Cys-374 in F-actin using fluorescence resonance energy transfer spectroscopy: effect of phalloidin on polymer assembly. *Biochemistry.* 33:13102–13108.
28. Wallrabe, H., M. Elangovan, A. Burchard, A. Periasamy, and M. Barroso. 2003. Confocal FRET microscopy to measure clustering of ligand-receptor complexes in endocytic membranes. *Biophys. J.* 85: 559–571.
29. Berney, C., and G. Danuser. 2003. FRET or no FRET: a quantitative comparison. *Biophys. J.* 84:3992–4010.
30. Frederix, P., E. L. d. Beer, W. Hamelink, and H. C. Gerritsen. 2002. Dynamic Monte Carlo simulations to model FRET and photobleaching in systems with multiple donor-acceptor interactions. *J. Phys. Chem. B.* 106:6793–6801.
31. Corry, B., D. Jayatilaka, and P. Rigby. 2005. A flexible approach to the calculation of resonance energy transfer efficiency between multiple donors and acceptors in complex geometries. *Biophys. J.* 89:3822–3836.
32. Lacowicz, J. R. 1999. Principles of Fluorescence Spectroscopy. Kluwer Academic/Plenum Press, New York.
33. Förster, T. 1949. Experimentelle und theoretische Untersuchung des Zwisschenenmolekularen ubergangs con Elektronenanregungserenrgie. *x. Naturforsch.* 4a:321–327.
34. Galanin, M. D. 1951. Quenching of solution fluorescence with absorbing substances. *Zhurn. Eksper. Teoret. Fiz.* 21:126–132.
35. Kurskii, A.Y., and A.S. Selivanenko. 1960. On the theory of luminescence quenching in liquid solutions. *Opt. Spectrosc.* 8:340–343.
36. Zimet, D. B., B. J. Thevenin, A. S. Verkman, S. B. Shohet, and J. R. Abney. 1995. Calculation of resonance energy transfer in crowded biological membranes. *Biophys. J.* 68:1592–1603.

37. Van Der Meer, B. W., I. G. Coker, and S.-Y. S. Chen. 1994. Resonance Energy Transfer: Theory and Data. VCH Publishers, Inc., New York.

38. Dictenberg, J. B., W. Zimmerman, C. A. Sparks, A. Young, C. Vidair, Y. X. Zheng, W. Carrington, F. S. Fay, and S. J. Doxsey. 1998. Pericentrin and gamma-tubulin form a protein complex and are organized into a novel lattice at the centrosome. *J. Cell Biol.* 141:163–174.

39. Kam, Z., T. Volberg, and B. Geiger. 1995. Mapping of adherens junction components using microscopic resonance energy transfer imaging. *J. Cell Sci.* 108:1051–1062.

40. Kindzelskii, A. L., Z. O. Laska, R. F. Todd III, and H. R. Petty. 1996. Urokinase-type plasminogen activator receptor reversibly dissociates from complement receptor type 3 ($\alpha_M\beta_2$, CD11b/CD18) during neutrophil polarization. *J. Immunol.* 156:297–309.

41. Heberle, F. A., J. T. Buboltz, D. Stringer, and G. W. Feigenson. 2005. Fluorescence methods to detect phase boundaries in lipid bilayer mixtures. *Biochim. Biophys. Acta.* 1746:186–192.

42. Plowman, S. J., C. Muncke, R. G. Parton, and J. F. Hancock. 2005. H-ras, K-ras, and inner plasma membrane raft proteins operate in nanoclusters with differential dependence on the actin cytoskeleton. *Proc. Natl. Acad. Sci. USA.* 102:15500–15505.

43. Dale, R. E., J. Eisinger, and W. E. Blumberg. 1979. The orientational freedom of molecular probes. The orientation factor in intramolecular energy transfer. *Biophys. J.* 26:161–193.

44. Corry, B., D. Jayatilaka, B. Martinac, and P. Rigby. 2006. Determination of the orientational distribution and orientation factor for transfer between membrane bound fluorophores using a confocal microscope. *Biophys. J.* 91:1032–1045.

45. Meyer, B. H., J. M. Segura, K. L. Martinez, R. Hovius, N. George, K. Johnsson, and H. Vogel. 2006. FRET imaging reveals that functional neurokinin-1 receptors are monomeric and reside in membrane microdomains of live cells. *Proc. Natl. Acad. Sci. USA.* 103:2138–2143.